

Provided for non-commercial research and education use.
Not for reproduction, distribution or commercial use.



This article appeared in a journal published by Elsevier. The attached copy is furnished to the author for internal non-commercial research and education use, including for instruction at the authors institution and sharing with colleagues.

Other uses, including reproduction and distribution, or selling or licensing copies, or posting to personal, institutional or third party websites are prohibited.

In most cases authors are permitted to post their version of the article (e.g. in Word or Tex form) to their personal website or institutional repository. Authors requiring further information regarding Elsevier's archiving and manuscript policies are encouraged to visit:

<http://www.elsevier.com/copyright>



Electrochromic nickel oxide/hydroxide thin films prepared by alternately dipping deposition

R. Cerc Korošec^{a,*}, J. Šauta Ogorevc^a, P. Draškovič^a, G. Dražić^b, P. Bukovec^a

^a Faculty of Chemistry and Chemical Technology, University of Ljubljana, Aškerčeva 5, SI-1000 Ljubljana, Slovenia

^b Jožef Stefan Institute, Jamova 39, SI-1001 Ljubljana, Slovenia

Received 1 April 2007; received in revised form 3 March 2008; accepted 11 March 2008

Available online 19 March 2008

Abstract

Nickel oxide/hydroxide thin films were prepared by alternately dipping deposition from NiSO₄ and LiOH solutions followed by heat-treatment. The onset temperature for nickel hydroxide decomposition was 220 °C for a thin film sample and 325 °C for the corresponding xerogel. During the decomposition nickel oxide was formed. The evolution of the infrared spectra during thermal decomposition is explained in detail. The thermally untreated xerogel contained sulfate ions, whereas in the thin sample they were replaced by carbonate ions originating from atmospheric CO₂. Optimization of the electrochromic response of thin films was performed using *in situ* spectroelectrochemical measurements. In the optimized film the degree of thermal decomposition of nickel hydroxide was 65% (120 min at 235 °C). The change in transmittance between the bleached and coloured state was low at the beginning of cycling (13% at $\lambda = 480$ nm), but increased during cycling and reached 45% in the 101st cycle (colouration efficiency -37 cm² C⁻¹). Transmission electron microscopy was used to examine the structure of the optimized film and of two more intensively thermally treated films. One of them (exposed to 300 °C for 24 h) became electrochemically active during cycling while the other (24 h at 400 °C) remained inert.

© 2008 Elsevier B.V. All rights reserved.

Keywords: Nickel oxide; Nickel hydroxide; Thin films; Electrochromism; Thermogravimetry; Alternately dipping deposition; Transmission electron microscopy; Optimisation

1. Introduction

Electrochromic nickel oxide thin films are good candidates for ion-storage materials in combination with tungsten oxide in complementary electrochromic devices [1]. Under anodic potentials NiO films change colour from transparent to deep brown. For chemically prepared NiO thin films the magnitude of the optical modulation during potential switching is crucially influenced by their heat-treatment, which is always performed after the deposition process [2–5]. For sol–gel prepared NiO films it has been shown that optimisation of thermal treatment on the basis of thermogravimetric (TG) analysis of the films assures higher coloration efficiency values, as well the stability of the film structure after prolonged cycling in an alkaline electrolyte [2,5,6].

Temperatures obtained for the corresponding xerogels are higher than for thin film samples by approximately 30 °C due to the difference in sample size. Therefore, optimisation and also explanation of the structural and morphological changes that occur during thermal treatment should be made on the basis of dynamic and isothermal TG measurements of thin films deposited on a substrate. The results show that each chemical system should be optimised separately regarding the preparation route [6].

The aim of our work was to investigate the temperature dependent electrochromic response of Ni(OH)_x thin films, prepared by the alternately dipping deposition (ADD) technique. Thermal decomposition of the film deposited on a substrate was compared to that of the xerogel. The difference of more than 100 °C between these two samples in the temperature at which NiO begins to form was explained with the help of Fourier transform infrared spectroscopy (FT-IR) of thermally untreated samples and intermediates formed during thermal decomposition. This study therefore

* Corresponding author.

E-mail address: romana.cerc-korosec@fkt.uni-lj.si (R. Cerc Korošec).

upgrades and completes work where thin film properties were explained by TG and X-ray diffraction (XRD) measurements of the corresponding xerogel [7].

2. Experimental details

2.1. Preparation of thin films and xerogels

Thin films were prepared on different substrates by the ADD technique. First, a wetting agent was dispersed on the substrate with a pulling velocity of 5 cm min^{-1} . For platinum foil and SnO_2/F glass, 1 wt.% of Teloxide (TEOL Factory, Ljubljana, Slovenia) in ethanol was used as the wetting agent, while for silicon resins 1 wt.% of Etolat (TEOL) in distilled water was used. After the wetting solution had dried, thin films were prepared by alternately immersing the substrates in two solutions, the first of 0.05 mol L^{-1} NiSO_4 (Kemika, Zagreb, Croatia) and the other of 0.05 mol L^{-1} LiOH (Kemika). Consequently a thin film of light green amorphous nickel hydroxide was formed on the substrate. The thickness of the thin film increased with the number of immersions, as noticed by observation. For TG measurements, thin films were deposited on platinum foil. For FT-IR analysis silicon resins polished on both sides were used as substrates. The number of immersions was 7 for each solution. For *in situ* spectroelectrochemical measurements, SnO_2/F glass was used as a substrate. The number of immersions was again 7. The xerogel used in TG and XRD measurements was obtained by mixing equal volumes of 0.1 M NiSO_4 and 0.1 M LiOH , centrifuged, cast in a Petri dish and dried in air at ambient temperature.

2.2. Instrumental

2.2.1. TG measurements

Thermoanalytical measurements were performed on a Mettler Toledo TG/SDTA 851^o instrument. In dynamic measurements, the temperature range from room temperature up to $900 \text{ }^\circ\text{C}$ was applied for the xerogel and thin films deposited on platinum foil. In isothermal measurements, the furnace was heated at 5° min^{-1} to the chosen temperature, left at that temperature for 180 min and then heated up to $400 \text{ }^\circ\text{C}$ at 5° min^{-1} . The baseline was subtracted in all cases. Xerogel intermediates used for FT-IR and XRD analyses were prepared in dynamic TG measurements up to the chosen temperature in the instrument itself. The thin films used for *in situ* spectroelectrochemical measurements were thermally treated in a large muffle furnace since the substrate was too heavy for heat-treatment in the TG instrument. It was not possible to increase the temperature in the muffle furnace linearly with time. It was therefore set to a predetermined isothermal temperature at which the films were thermally treated for a certain time. Isothermal TG measurements of films deposited on platinum substrates were performed in advance to determine the degree of thermal decomposition of the films exposed to isothermal conditions. The procedure is described in detail in connection with Fig. 3. From the ratio of the isothermal weight loss after a defined time and the weight loss associated with the decomposition of anhydrous nickel hydroxide, which for thin films was complete at $400 \text{ }^\circ\text{C}$, the degree of thermal decomposition could be estimated [2].

2.2.2. Evolved gas analysis (EGA)

Thermogravimetry-mass spectroscopy (TG-MS) is a coupled technique which enables determination of the nature and the amount of volatile product or products formed during thermal decomposition [8]. TG-MS measurement of the xerogel was performed on a STA 409 Netzsch apparatus. Evolved gases were detected using a Leybold Heraeus Quadrex 200 mass spectrometer which was connected to the exhaust line of the TG instrument via a 75 cm long heated leak. During measurement the furnace was purged with air (100 mL min^{-1}). The heating rate was 5 K min^{-1} .

2.2.3. XRD analysis

Powder diffraction data of xerogel samples were obtained using a PANalytical X'Pert PRO diffractometer with $\text{Cu K}\alpha$ radiation from 5 to 80 2θ in steps of 0.04 and a time per step of 1 s^{-1} .

2.2.4. FT-IR measurements

Fourier transform infrared (FT-IR) spectroscopic measurements were made using a Perkin Elmer System 2000 spectrophotometer with a resolution of 4 cm^{-1} . To obtain the transversal optical modes, films were deposited on Si wafers. Thermal treatment of thin films heat-treated to different degrees was performed as a dynamic measurement using the TG instrument. For xerogel measurements KBr pellets embedding xerogels were prepared. Intermediates of xerogel and the thin film were heated to different temperatures which are marked in Fig. 1 with stars.

2.2.5. Spectroelectrochemical measurements

In situ UV–VIS spectroelectrochemical measurements were made in the range 360 – 1100 nm using a Perkin Elmer UV/VIS Lambda 2 Spectrometer, connected to an EG&G PAR Model 273 computer-controlled potentiostat–galvanostat. A potential scan rate of 10 mV s^{-1} was used for CV measurements. A homemade three-electrode spectroelectrochemical transmission cell, filled with 40 mL of 0.1 M LiOH , was used. A Pt rod served as the counter electrode, an $\text{Ag/AgCl/KCl}_{\text{sat}}$ cell as the reference electrode ($E=0.197 \text{ V}$) and a thin Ni-oxide film deposited on SnO_2/F

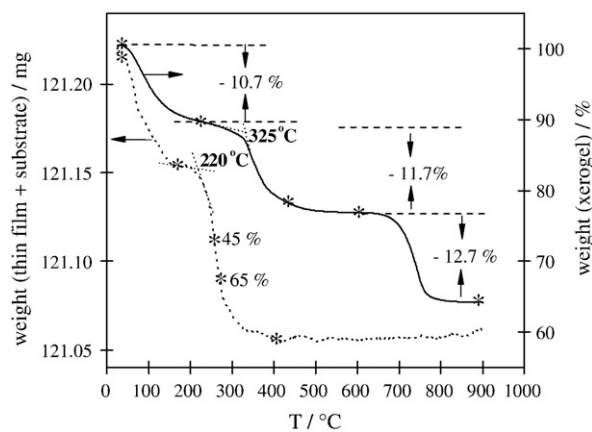


Fig. 1. Dynamic TG curves of a thin film (left ordinate) and of the powder (right ordinate) in a dynamic air atmosphere. The initial weight of the thin film and substrate was 121.218 mg , while that of the powder was 9.880 mg . IR analysis was performed for the intermediates marked in Fig. 1 with stars.

glass (square resistivity $13 \Omega/\delta$) as the working electrode. For background measurements, a cell filled only with electrolyte was used.

2.2.6. Transmission electron microscopy (TEM) study

For the TEM study a cross section of the sample on a <Si> substrate was prepared using an adapted Gatan cross-sectional TEM specimen preparation kit. After mechanical thinning and dimpling, ion milling using 3.8 keV argon ions at a 10° incident angle was used. Samples were examined by a JEOL 2010 F transmission electron microscope, operated at 200 kV. The chemical composition of the phases was determined using a Link ISIS-300 energy dispersive X-ray spectroscopy (EDXS) system from Oxford Instruments with an ultra-thin window Si(Li) detector. Spectra were collected using a 200 keV electron beam with a collection time of 100 s. Spectra were collected in the energy range up to 20 keV. During EDXS analysis special care was taken to prevent beam-induced specimen damage, so we normally used a 50 μm condenser aperture, spot size 3 and a beam diameter larger than 20 nm.

3. Results and discussion

A comparison of dynamic TG measurements of a thin film deposited on a Pt foil, and the corresponding xerogel is presented in Fig. 1. Comparison of the dynamic TG curve of the xerogel with the published one [7] shows that there is some discrepancy in weight loss (Table 1), while the temperature range of the separate steps is very similar. The reason for the discrepancy is probably the different chemical compositions caused by the different precipitation solution (we used LiOH while the authors [7] used KOH) on the one hand, and the lower moisture content in our sample on the other. However, there is a great difference in the course of thermal decomposition of the thin film sample (dotted curve) with respect to that of the xerogel (solid curve). The first step in the weight loss curve is ascribed to dehydration of adsorbed water and elimination of intercalated water, and this occurred for both samples up to 200 °C. Then the thermal decomposition of nickel hydroxide to nickel oxide began according to the reaction $\text{Ni}(\text{OH})_2 \rightarrow \text{NiO} + \text{H}_2\text{O}$, which is evident from the second step of the TG curve. Nickel hydroxide exists in two polymorphic forms: crystallized β - $\text{Ni}(\text{OH})_2$ and α - $\text{Ni}(\text{OH})_2$, which is used to denominate a large set of disordered Ni(II) hydroxides with low crystallinity and an excess of intersheet water and foreign ions [9]. During their

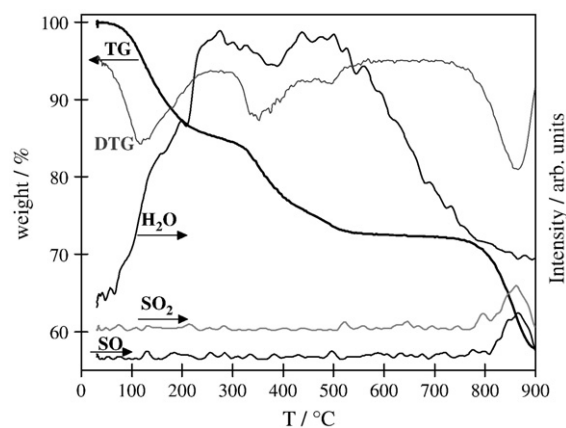


Fig. 2. TG and EGA-MS curves of the xerogel.

precipitation from aqueous salt solution, poorly crystallized α -type hydroxides or hydroxy-salts can be isolated. In our case an amorphous product was obtained, as evident from the XRD spectrum of the thermally untreated xerogel. For β - $\text{Ni}(\text{OH})_2$ it was already shown that from room temperature up to 250 °C dehydration takes place and above this temperature decomposition of $\text{Ni}(\text{OH})_2$ occurs [10,11].

Thermal decomposition of the thin film started at a temperature 100 °C lower (220 °C) than that of the corresponding xerogel (325 °C). It is known that in dynamic measurements the decomposition temperature decreases with decrease in sample particle size [12] since decomposition products first have to diffuse to the surface of the solid particle before they evolve. This process takes longer in the case of larger particles, while the temperature in dynamic measurements is increasing. Therefore decomposition temperatures for xerogel samples with an average size of some μm are shifted towards higher values in comparison with thin films with a thickness of some tens of a nm. On the basis of our previous examination this temperature difference was around 30 °C [6], so we concluded that there should be another reason in this case for such a large difference in the thermal stability of the precipitated $\text{Ni}(\text{OH})_x$ thin film with respect to the xerogel, most probably the different counter-ion. Lithium and sulfate ions are present in the structure due to the mode of preparation of the sample. Comparison of the IR spectra for the thin film and the xerogel showed that there is a large amount of sulfate ions in the xerogel sample, while in the thin film sample carbonate ions are predominant. The origin of the carbonate ions is from atmospheric CO_2 which chemisorbed on the basic surface after the thin film has been lifted from the LiOH solution. Reichle [13] reported that in layered hydroxides the order of affinity towards anions is: $\text{CO}_3^{2-} > \text{SO}_4^{2-}$, $\text{OH}^- > \text{F}^- > \text{Cl}^-$. During the ADD process the excess of negative sulfate ions (caused by carbonate insertion) precipitated in the thin film must return to the solution due to the electroneutrality condition. For the bulk material (xerogel) no evident insertion of carbonate ions took place. The reason is that the huge surface area of the amorphous $\text{Ni}(\text{OH})_x$ precipitated on the substrate acts as a nanostructured material. Many of the atoms are on the surface, allowing a nearly stoichiometric surface–gas reaction [14]. Carbonates are less thermally stable than sulfates. The mixture of NiCO_3 and $\text{Ni}(\text{OH})_2$ thermally decomposed at

Table 1
Comparison of weight loss between a xerogel prepared from KOH [7] and from LiOH

	Weight loss / %		
	1st step (25—approx. 200 °C)	2nd step (200—approx. 600 °C)	3rd step (600—approx. 900 °C)
Xerogel [7], precip. agent KOH	15.8	17.9	8.9
Xerogel, precip. agent LiOH	10.7	11.7	12.7

400 °C, while thermal decomposition of NiSO₄ was complete at 900 °C [15]. Sulfate ions in the xerogel therefore stabilized the Ni(OH)₂ structure and decomposition began at higher temperature. The third step in the TG curve of the xerogel above 600 °C is a result of the decomposition of NiSO₄ to NiO. On the TG–MS curve (Fig. 2) this is confirmed by the release of SO (mass peak 48) and SO₂ (mass peak 64). The mass peak of released water is shifted towards a higher temperature with regard to the derivative TG (DTG) curve and its resolution is also poorer. The reason is that the mass spectrometer is connected to the thermoanalyser via a heated capillary 75 cm long and therefore a certain time shift during evolution of gas species and their detection in the mass spectrometer is observed.

Fig. 3a and b presents the isothermal TG curve at 220 °C of a thin film deposited on a Pt foil. In Fig. 3a the temperature profile in the furnace is presented on the right-hand axis and on the left-hand the weight of the film on the substrate in a percentage scale. The first step in the TG curve occurred during linear heating and is due to dehydration. Thermal decomposition of nickel hydroxide to oxide occurs after the furnace reaches its isothermal temperature and is fast in the beginning, but becomes slow with increasing time. After 120 min the decomposition of anhydrous hydroxide to oxide reaches 60%, as marked in Fig. 3b, which represents the temperature dependence of the same data. The temperature in the furnace was increased again after 180 min at 220 °C to a final temperature of 400 °C, where decomposition to nickel oxide was complete (100%).

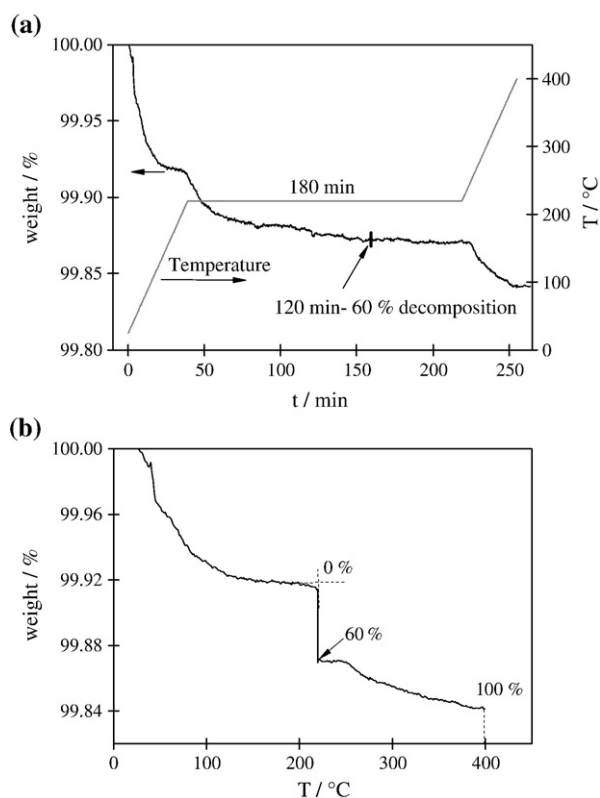


Fig. 3. Isothermal TG curves of a thin film deposited on a platinum foil at 220 °C; time dependence (a) and temperature dependence (b).

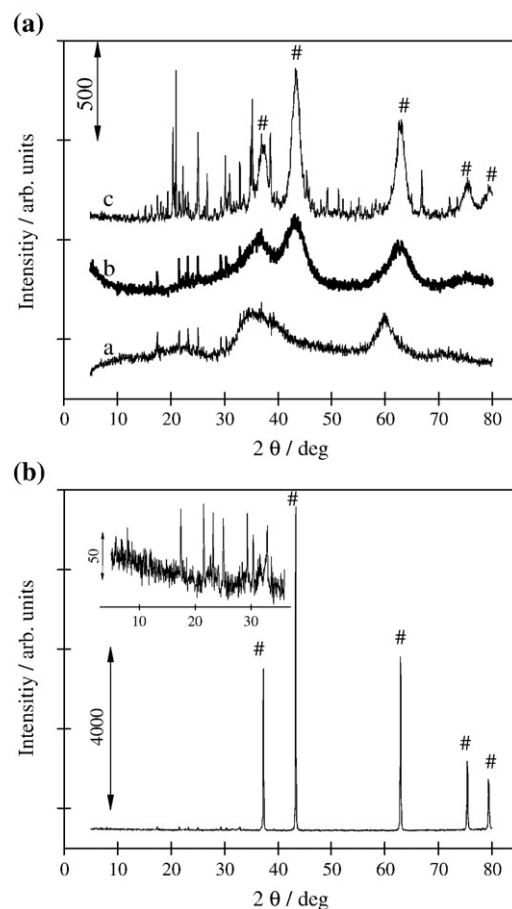


Fig. 4. XRD spectra of xerogel intermediates: xerogel treated up to 200 °C—(a); 400 °C—(b); 600 °C—(a) and to 900 °C (b).

In Fig. 4a and b evolution of the XRD spectra of the xerogel with increasing temperature is presented. The xerogel, heat-treated to 200 °C, showed the diffraction profile of an amorphous material. The sharp peaks appearing at lower angles from approximately 15 to 35 2θ indicate the presence of LiSO₄·H₂O (PDF 15-873) [16]. On heating to 400 °C, nickel oxide crystallites were formed. The intermediate at 600 °C is a mixture of NiO, which is still not well crystallised (marked in Fig. 4a with #, PDF 65-6920), two polymorphs of NiSO₄·6H₂O (PDF 47-1811 and 79-1654), anhydrous NiSO₄ (PDF 72-1242) and LiSO₄·H₂O. At 900 °C a mixture of crystallized nickel oxide and a small amount of LiSO₄·H₂O is obtained (Fig. 4b). This means that sulfate ions coordinated to nickel thermally decompose between 600 and 800 °C, but those coordinated to lithium still remain in the structure as lithium sulfate is thermally stable up to 860 °C [17]. The identified hydrated phases mean that between the TG and XRD measurements rehydration of the samples occurred.

The evolution of IR transmittance spectra during heat-treatment of the xerogel is shown in Fig. 5. The presence of water molecules in the thermally untreated xerogel is revealed by a broad band positioned between 3800 and 2800 cm⁻¹, which belongs to the $\nu(\text{O-H})$ stretching vibrations. The band is broadened due to hydrogen bonds. The band at 1630 cm⁻¹ is characteristic of the bending vibration of water. The intense peak

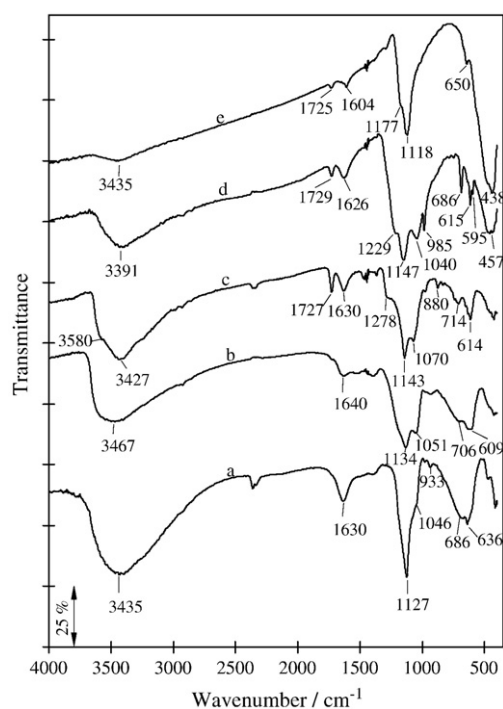


Fig. 5. IR transmittance spectra of xerogel intermediates: thermally untreated xerogel—a; xerogel treated up to 220 °C—b; 400 °C—c; 600 °C—d and 900 °C—e.

positioned at 1127 cm^{-1} corresponds to stretching vibrations of free sulfate ions with T_d symmetry, meaning that a large amount of sulfate ions are intercalated in the structure. The shoulder at 1046 cm^{-1} and splitting of the peak in the region of the bending modes of sulfate ions ($686, 636\text{ cm}^{-1}$) are characteristic of monodentate coordination [18]. The ratio between the intensity of the peaks positioned at 1134 and 1051 cm^{-1} changed in the xerogel thermally treated up to 220 °C , so we assume that there are more monodentately coordinated sulfate ions in this sample. On further thermal treatment, dehydroxylation of $\text{Ni}(\text{OH})_2$ occurs leading to NiO formation. Up to 400 °C this process is not complete (Fig. 1) and the $\text{Ni}-\text{O}$ stretching vibration (438 cm^{-1}) is not yet pronounced. Small NiO crystallites possess a large surface area. The band at 1727 cm^{-1} is attributed to vibrations of the carbonate ions that are bridge-bonded to the surface of NiO grains [19]. The band at 1278 cm^{-1} belongs to the combination of stretching and bending vibrations of bidentately coordinated carbonate ions [20]. Most probably they originate from atmospheric CO_2 . The shoulder at 3580 cm^{-1} indicates the presence of non-hydrogen bonded OH group. In the spectrum of the xerogel thermally treated to 600 °C , which is a mixture of several sulfates (see XRD spectrum, Fig. 4a), the symmetry of sulfate groups was lowered to C_{2v} , which corresponds to bidentate and bridge-bonded coordination. The band for stretching $\text{Ni}-\text{O}$ vibrations is the strongest in the spectrum of the xerogel treated up to 900 °C . Sulfate ions are still present in the structure due to the presence of $\text{LiSO}_4 \cdot \text{H}_2\text{O}$.

IR spectra of thin films deposited on silicon resin and thermally treated to different extents are shown in Fig. 6. In the IR spectrum of the thermally untreated thin film the bands at $1488, 1419$ and

861 cm^{-1} represent stretching vibrations of the adsorbed carbonate ion, which is planar and has D_{3h} symmetry ($\nu_2(\text{CO}_3^{2-}) = 879\text{ cm}^{-1}$; $\nu_3(\text{CO}_3^{2-}) = 1429$ and 1492 cm^{-1}). The band at 1588 cm^{-1} arises from the stretching $\text{C}-\text{O}$ vibrations of the bidentately coordinated carbonate ion [18]. The band at 667 cm^{-1} arises from the bending vibration of $\delta(\text{Ni}-\text{OH})$. After dehydration the shape of the spectrum resembles to the spectrum of a layered turbostratic $\text{Ni}(\text{OH})_2$ [9], on which vibrations of carbonate ions are superimposed. With a higher degree of thermal decomposition, the band for stretching $\text{Ni}-\text{O}$ vibrations becomes more and more intense. The intensities of bands for carbonate ions diminish during heat-treatment. Besides the intense $\text{Ni}-\text{O}$ stretching vibration, there are two peaks due to adsorbed moisture and a peak of the silicon substrate (1088 cm^{-1}) in the spectrum of the film thermally treated up to 400 °C .

In situ monochromatic optical transmittance changes ($\lambda = 480\text{ nm}$) during chronocoulometric measurements of thin films thermally treated to different degrees are shown in Fig. 7. Fig. 7a represents the response at the beginning of the cycling experiment, while 7b shows the stabilised 101st cycle during charging at a potential of 0.6 V vs. Ag/AgCl ($0-30\text{ s}$) and discharging at 0.0 V vs. Ag/AgCl ($30-60\text{ s}$). At the beginning of cycling, the highest degree of coloration was shown by the thin film where the degree of thermal decomposition from amorphous anhydrous nickel hydroxide to oxide was 25% (120 min at 215 °C). After prolonged cycling the decrease of transmittance in its bleached state of 15% indicated that the colouring/bleaching process is not reversible. The change in transmittance during the 2nd coloration was only 15% for a thin film exposed

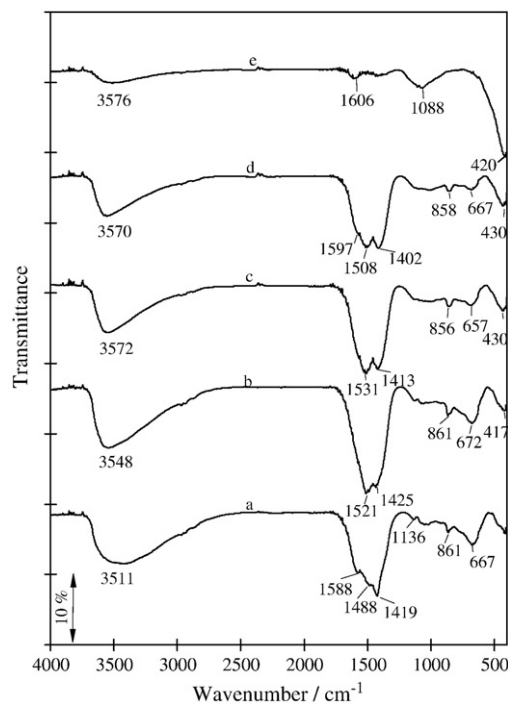


Fig. 6. IR transmittance spectra of thin films thermally treated to different degrees: thermally untreated film—a; film after dehydration (dynamically up to 160 °C)—b; film with 45% decomposition (up to 255 °C)—c; 65% decomposition (up to 270 °C)—d and 100% decomposition (up to 400 °C)—e.

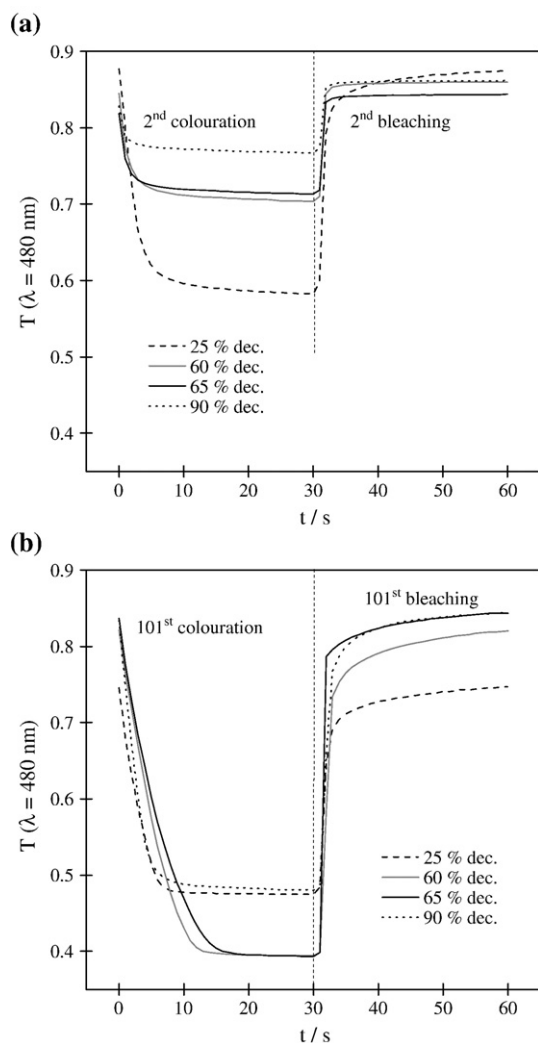


Fig. 7. *In situ* monochromatic optical transmittance changes ($\lambda=480$ nm) during chronocoulometric measurements of thin films thermally treated to different degrees (2nd cycle—(a), 101st cycle—(b)). The films were coloured at 0.6 V for 30 s and bleached at 0.0 V for 30 s.

for 120 min at 220 °C (60% decomposition), but in the 101st cycle it reached a better value (43%) than the film with 25% decomposition (27%). After the 101st bleaching process, the decrease in transmittance showed that reversibility was not yet achieved (Fig. 7b). An optimal optical response in the 101st cycle was exhibited by the film with 65% decomposition (120 min at 235 °C); the calculated coloration efficiency (CE) reached -37 cm² C⁻¹, while at the beginning of cycling CE was -32 cm² C⁻¹. For more thermally treated films the optical modulation was lower with regard to the optimized film. From Fig. 7b we can see that it took around 5 s to colour the film with 25% decomposition and 90% decomposition, while films with 60 and 65% decomposition needed more time (approx. 15 s). The reason probably lies in the different structures of these films.

The evolution of the cyclic voltammetric curves and the corresponding *in situ* monochromatic transmittance changes of the optimized film (65% decomposition—120 min at 235 °C) are shown in Fig. 8a and b. This film exhibited excellent reversibility in the 101st cycle. At the beginning of cycling the

basic form of the cyclic voltammetric curve was not yet developed (Fig. 8a). During the cycling process current densities became larger. The anodic and cathodic peaks became more and more pronounced, and the potential difference between them larger, indicating loosening of the structure. The changes in transmittance between the bleached and coloured state increased from 13% in the 1st cycle to 45% in the 100th cycle.

In Fig. 9 TEM micrographs of thin films thermally treated for 120 min at 235 °C (65% decomposition—a1, a2), for 24 h at 300 °C (b1, b2) and 24 h at 400 °C (c1, c2) are shown. We compared the microstructure of the optimized film with the microstructure of a film which became electrochemically active after prolonged cycling in alkaline electrolyte and one which stayed totally inactive [7]. The microstructure of the optimized film is not as well developed as in the case of the films prepared by the sol–gel method [21]. It consists of particles (flakes) with a size from 20 to 50 nm, and there is also some inner porosity. The open porosity of this sample enabled diffusion of LiOH during the cycling process through the whole thickness of the layer. From the FT-IR spectrum it is evident that the film consists of two

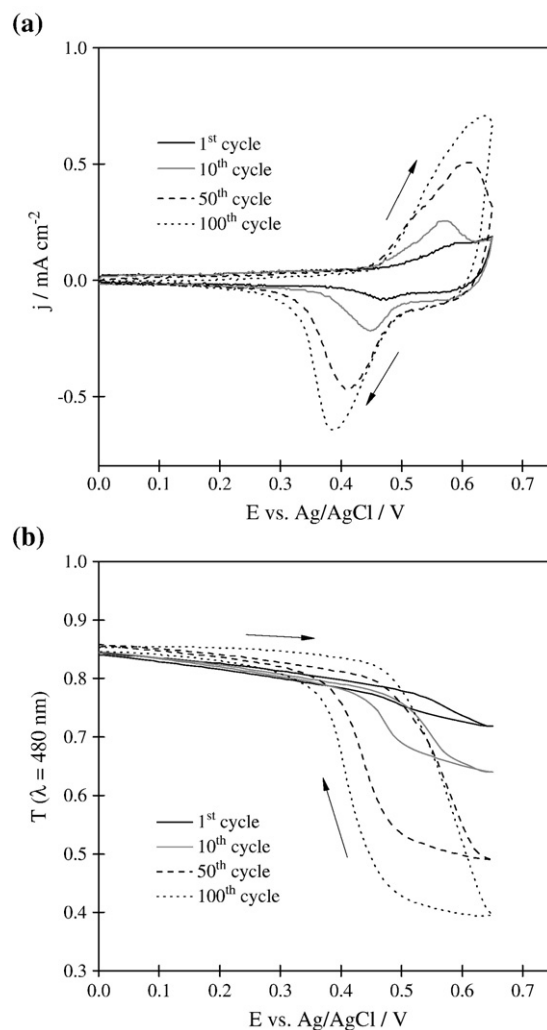


Fig. 8. Cyclovoltammetric curves (a) and monochromatic transmittance changes (b) of the optimized film (65% decomposition—120 min at 235 °C).

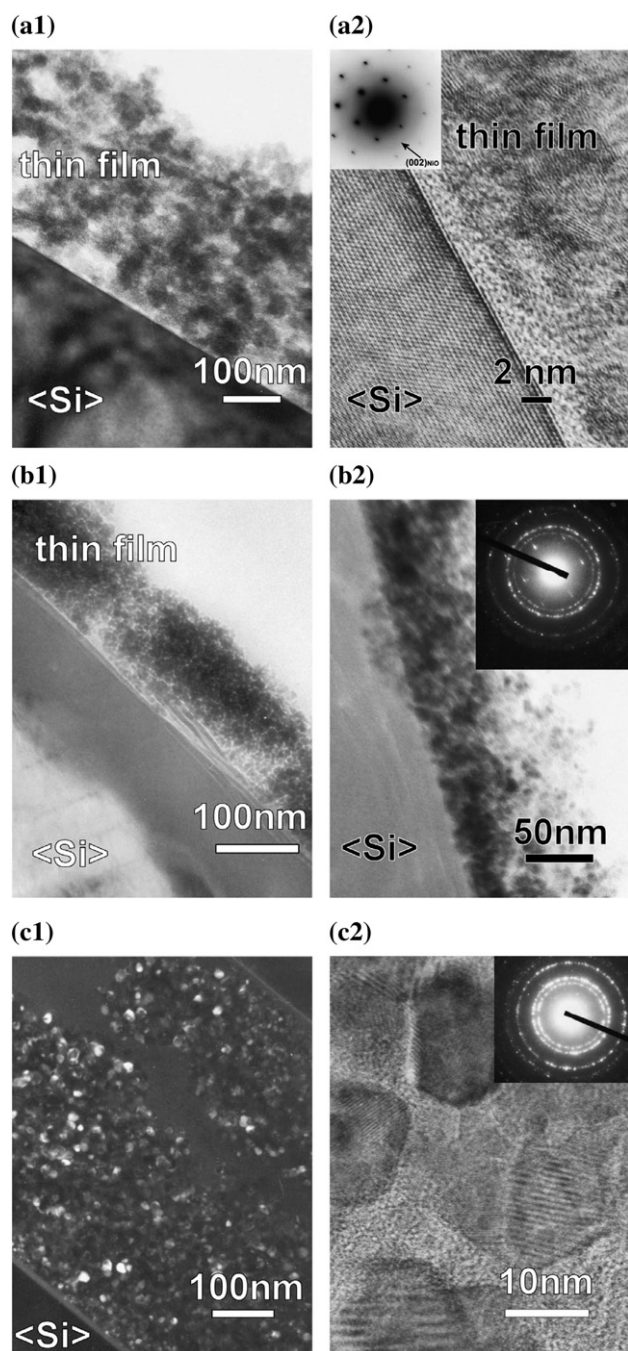


Fig. 9. TEM micrographs of the optimised film (65% decomposition: 120 min at 235 °C—9a1 and 9a2), film exposed for 24 h to 300 °C—9b1 and 9b2 and for 24 h to 400 °C—9c1 and 9c2.

structures: nickel hydroxide with inserted and bidentately coordinated carbonate ions and nickel oxide. The thickness of the film is around 300 nm (Fig. 9a1). The high-resolution TEM (HRTEM) image and the Selected Area Electron Diffraction (SAED) pattern (Fig. 9a2 with inset) of a cross section of the thin film show that the film is composed of an amorphous phase and a few nanometre (2–3 nm) sized crystalline particles. In the SAED pattern, where the well defined diffraction spots originate from the silicon substrate, the faint and diffuse circle corresponds to the (002) plane of cubic NiO (marked with an arrow). Between the

silicon monocrystalline substrate and the NiO nanoparticles there is a continuous amorphous layer around 2 nm thick, indicating that the NiO particles were formed during heat-treatment by homogeneous nucleation. The estimated thickness of the film, annealed for 24 h at 300 °C (100% decomposition), is 130 nm (Fig. 9b1); that is more than twice as thin as the previously described film. That means that there is a considerable variation of film thickness in the sample. The size of the nickel oxide grains is 5 nm. This film was inactive at the beginning of cycling, but during the cycling process became more and more active [7]. In Fig. 9c1 (dark-field) and 9c2 (high-resolution) TEM micrographs of the film which stayed inactive during the cycling experiment are shown. Fig. 9c1 (two different parts of the film sample are shown together) again confirms that there is a great variation of film thickness, reaching 175 nm on one part and 350 nm on the other. Heat-treatment at 400 °C for 24 h resulted in the formation of larger grains of nickel oxide. The average diameter of the well crystallized (shaped) NiO grains is 10 nm, as can be seen from the image on Fig. 9c2. The grains are embedded in an amorphous matrix and overlap each other, producing characteristic Moiré patterns in the HRTEM image (bright and dark fringes in overlapping areas).

4. Conclusion

Comparison of dynamic TG measurements made on ADD prepared thin films and the corresponding xerogels suggested that the two samples differ in more than sample size. The observed difference in onset decomposition temperature of nickel hydroxide was more than 100 °C. For sol–gel prepared samples the difference in onset decomposition temperature was around 30 °C [6]. Besides, the xerogel sample exhibited a third step in the dynamic TG curve in the range from 600 to 800 °C, while the TG curve of the thin film was flat in this range. With the help of FT-IR spectroscopy it was found that sulfate ions were replaced by carbonate ions in thin film samples, most probably during the ADD process when the sample was repeatedly pulled out of the solution. At that time, atmospheric CO₂ reacted with hydroxide ions leading to carbonate formation. We conclude that all sulfate ions were exchanged by carbonate ones since in the FT-IR spectrum there is no evidence of sulfate vibrations. Sulfate ions returned to solution but we did not investigate the mechanism of this process. For the xerogel sample, which we prepared by mixing equal volumes of the two solutions, this process could not happen.

The film where decomposition of nickel hydroxide was 65% possessed an optimised electrochromic response up to 101st cycle. From the FT-IR spectrum it is evident that it was composed of two structures: layered nickel hydroxide with inserted and bidentately coordinated carbonate ions and nickel oxide. The TEM micrograph showed a thin film with a thickness of 300 nm which consisted of flakes 20–50 nm in size. Inside the flakes NiO nanoparticles (2–3 nm in diameter) were embedded in an amorphous matrix (Fig. 9a1 and 9a2). Optical modulation of less thermally treated films was better at the beginning of cycling, but poorer in the 101st cycle with regard to the optimized film. The bleaching process was not reversible, and the coloration less intensive than for the optimized film. Optical modulation of more

thermally treated films (>65%) was lower with regard to the optimized film (Fig. 7b). In our previous work we already noticed that thermal decomposition of sol–gel prepared films which contain carbonate ions are always lower than in the case of sulfate ions [6]. Carbonates probably hold the amorphous structure tightly together. Consequently they are hardly exchanged with OH^- to obtain an electrochromically active $\text{Ni}(\text{OH})_2$ phase, leading to poorer response at the beginning of cycling. TEM showed that the performance of films which consisted of only NiO phase (100% decomposition) depended on the grain size and crystallinity. In the case when the size of the nanograins reached 5 nm in diameter, the film became electrochemically/electrochromically active during cycling. After 14 h the change in transmittance between the coloured and bleached state reached 30% [7]. A film of 10 nm NiO grain size remained electrochemically inert, probably due to its lower active surface size on one hand, and to the increase in crystallinity on the other.

References

- [1] A. Azens, C.G. Granqvist, *J. Solid State Electrochem.* 7 (2003) 64.
- [2] R. Cerc Korošec, P. Bukovec, B. Pihlar, J. Padežnik Gomilšek, *Thermochim. Acta* 402 (2003) 57.
- [3] A. Šurca, B. Orel, B. Pihlar, P. Bukovec, *J. Electroanal. Chem.* 408 (1996) 83.
- [4] X. Chen, X. Hu, J. Feng, *Nanostruct. Mater.* 6 (1994) 309.
- [5] R. Cerc Korošec, P. Bukovec, *Thermochim. Acta* 410 (2004) 65.
- [6] R. Cerc Korošec, P. Bukovec, *Acta Chim. Slov.* 53 (2006) 136.
- [7] M.C.A. Fantini, G.H. Bezerra, in: C.M. Lampert, C.G. Granqvist (Eds.), *Optical Materials Technology for Energy Efficiency and Solar Energy Conversion X*, San Diego, U.S.A., July 25–26, 1991, SPIE Proceedings, vol. 536, 1991, p. 81.
- [8] J. Mullens, in: M.E. Brown, P.K. Gallagher (Eds.), *Handbook of Thermal Analysis and Calorimetry, Principles and Practice*, Vol. 1, Elsevier, Amsterdam, 1998, p. 509.
- [9] P. Oliva, J. Leonardi, J.F. Laurent, C. Delmas, J.J. Braconnier, M. Figlarz, F. Filvet, *J. Power Sources* 8 (1982) 229.
- [10] T.S. Horányi, *Thermochim. Acta* 137 (1989) 247.
- [11] Q. Song, Z. Tang, H. Guo, S.L.I. Chan, *J. Power Sources* 112 (2002) 428.
- [12] W.W. Wendlandt, *Thermal Methods of Analysis*, Interscience Publishers, New York, 1964, p. 17.
- [13] W.T. Reichle, *Solid State Ionics* 22 (1986) 135.
- [14] K.J. Klabunde, R.S. Mulukutla, in: K.J. Klabunde (Ed.), *Chemical and Catalytic Aspects of Nanocrystals, Nanoscale Materials in Chemistry*, Wiley, New York, 2001, p. 223.
- [15] *Atlas of Thermoanalytical Curves*, in: G. Liptay (Ed.), Akadémiai Kiadó Budapest, 1977, Vol. 5.
- [16] *Powder Diffraction File-4-Release*, in: W.F. McClune (Ed.), International Centre for Diffraction Data, Newtown Square, PA, 2006.
- [17] P. Bukovec, N. Bukovec, in: Ž.D. Živković (Ed.), *Thermal Analysis, Collection of Papers*, Bor, Yugoslavia, 1984.
- [18] K. Nakamoto, *Infrared and Raman Spectra of Inorganic and Coordination Compounds*, 5th Ed. John Wiley & Sons, New York, 1997.
- [19] G. Busca, V. Lorenzelli, *Mater. Chem.* 7 (1982) 89.
- [20] M. Figlarz, S. Le Bihan, *C. R. Acad. Sci.*, 272 (1971) 580.
- [21] R. Cerc Korošec, P. Bukovec, B. Pihlar, A. Šurca Vuk, B. Orel, G. Dražič, *Solid State Ionics* 165 (2003) 191.